Decisive disappearance search at high Δm^2 with monoenergetic muon neutrinos

S. Axani,[1] G. Collin,[1] J. M. Conrad,[1] M. H. Shaevitz,[2] J. Spitz,[1] and T. Wongjirad[1]

[1]*Massachusetts Institute of Technology, Cambridge, Massachusetts 02139, USA*
[2]*Columbia University, New York, New York 10027, USA*

"KPipe" is a proposed experiment which will study muon neutrino disappearance for a sensitive test of the $\Delta m^2 \sim 1$ eV^2 anomalies, possibly indicative of one or more sterile neutrinos. The experiment is to be located at the J-PARC Materials and Life Science Experimental Facility's spallation neutron source, which represents the world's most intense source of charged kaon decay-at-rest monoenergetic (236 MeV) muon neutrinos. The detector vessel, designed to measure the charged-current interactions of these neutrinos, will be 3 m in diameter and 120 m long, extending radially at a distance of 32 to 152 m from the source. This design allows a sensitive search for ν_μ disappearance associated with currently favored light sterile neutrino models and features the ability to reconstruct the neutrino oscillation wave within a single, extended detector. The required detector design, technology, and costs are modest. The KPipe measurements will be robust since they depend on a known energy neutrino source with low expected backgrounds. Further, since the measurements rely only on the measured rate of detected events as a function of distance, with no required knowledge of the initial flux and neutrino interaction cross section, the results will be largely free of systematic errors. The experimental sensitivity to oscillations, based on a shape-only analysis of the L/E distribution, will extend an order of magnitude beyond present experimental limits in the relevant high-Δm^2 parameter space.

I. INTRODUCTION

A number of experimental anomalies consistent with neutrino oscillations at a characteristic mass splitting around 1 eV^2 hint at the possibility of an additional neutrino. These anomalies fall into two categories: muon-to-electron flavor appearance, as observed by the LSND [1] and MiniBooNE [2,3] experiments, and electron flavor disappearance, as observed by reactor [4,5] and source [6–9] experiments. A favored beyond the standard model explanation for these anomalies invokes an additional number of N sterile neutrinos participating in oscillations beyond the three active flavors [10–13]. These "$3 + N$ models" can be used to simultaneously describe the existing anomalous observations and those measurements which do not claim a signal in the relevant parameter space [14–22]. The presence of eV-scale sterile neutrinos also influences the evolution of the early Universe, which makes understanding the constraints cosmological data have on $3 + N$ models a highly active area of research and debate (e.g. [13,23,24]). In this work, we limit the scope to laboratory experiments, where $3 + N$ fits to the data exhibit tensions between both neutrino and antineutrino measurements and appearance and disappearance measurements.

Muon neutrinos must disappear if the observed anomalies are due to oscillations involving a light sterile neutrino. In order to understand the importance of ν_μ disappearance measurements, consider the short-baseline approximation

for a $3 + 1$ sterile neutrino model with mass eigenstates $m_1 \approx m_2 \approx m_3 \ll m_4$, where m_{1-3} represent the active mass states and m_4 the sterile state. The probability for $\nu_\mu \rightarrow \nu_e$ appearance is given by

$$P(\nu_\mu \rightarrow \nu_e) \simeq 4|U_{\mu 4}|^2|U_{e4}|^2\sin^2(1.27\Delta m_{41}^2 L/E). \quad (1)$$

The probability for ν_e and ν_μ disappearance are, respectively,

$$P(\nu_e \rightarrow \nu_e) \simeq 1 - 4(1 - |U_{e4}|^2)|U_{e4}|^2\sin^2(1.27\Delta m_{41}^2 L/E) \quad (2)$$

and

$$P(\nu_\mu \rightarrow \nu_\mu) \simeq 1 - 4(1 - |U_{\mu 4}|^2)|U_{\mu 4}|^2\sin^2(1.27\Delta m_{41}^2 L/E). \quad (3)$$

In these equations, the elements of the mixing matrix, U, set the amplitude of oscillation, while Δm_{41}^2 establishes the oscillation wavelength. Within this $3 + 1$ model, a global fit to the world's data, including all anomalies and null results, will simultaneously constrain U_{e4}, $U_{\mu 4}$, and Δm_{41}^2. The range of values that $U_{\mu 4}$ can take on, and therefore the oscillation parameters that govern ν_μ disappearance, can thus be restricted. The present global fit for ν_μ disappearance places the allowed region just outside of current

bounds. This motivates the construction of a fast, low cost [25], and decisive ν_μ disappearance experiment that can confirm or disallow various models for sterile neutrinos, as well as inform a range of future proposed experiments [24,26–34].

In what follows we describe such an experiment, called KPipe, that can perform a search for ν_μ disappearance that extends well beyond current limits while still being low cost. KPipe will employ a long, liquid scintillator-based detector that is oriented radially with respect to an intense source of isotropic monoenergetic 236 MeV ν_μs coming from the decay at rest (DAR) of positively charged kaons ($K^+ \rightarrow \mu^+ \nu_\mu$; BR $= 63.55 \pm 0.11\%$ [35]). As the only relevant monoenergetic neutrino that can interact via the charged-current (CC) interaction, a kaon decay-at-rest (KDAR) ν_μ source represents a unique and important tool for precision oscillation, cross section, and nuclear physics measurements [36,37]. Since the energy of these neutrinos is known, indications of ν_μ disappearance may be seen along the length of the KPipe detector as oscillating deviations from the expected $1/R^2$ dependence in the rate of ν_μ CC interactions. A measurement of such a deviation over a large range of L/E would not only be a clear indication for the existence of at least one light sterile neutrino, but also begin to disambiguate among different sterile neutrino models.

II. THE KDAR SOURCE AND KPIPE DETECTOR DESIGN

The Materials and Life Science Experimental Facility (MLF) at the Japan Proton Accelerator Research Complex (J-PARC) in Tokai, Japan houses a spallation neutron source used for basic research on materials and life science, as well as research and development in industrial engineering. It is also an intense, yet completely unutilized, source of neutrinos that emits the world's most intense flux of KDAR monoenergetic (236 MeV) ν_μs. Neutrinos from pions, muons, and kaons are generated when a mercury target is hit by a pulsed, high intensity proton beam from the J-PARC rapid-cycling synchrotron (RCS) [30]. The RCS delivers a 3 GeV, 25 Hz pulsed proton beam, which arrives in two 80 ns buckets spaced 540 ns apart. The facility provides users 500 kW of protons on target (POT) but has demonstrated its eventual steady-state goal of 1 MW, albeit for short times [38]. The proton-on-target interaction provides an intense source of light mesons, including kaons and pions, which usually come to rest in the high-A target and surrounding shielding.

KPipe will search for muon-flavor disappearance with CC interactions of 236 MeV ν_μs on carbon nuclei ($\nu_\mu\,^{12}\mathrm{C} \rightarrow \mu^- X$) in liquid scintillator. This interaction produces a visible muon and X, where X is some combination of an excited nucleus, deexcitation photons, and one or more ejected nucleons after final state interactions. The
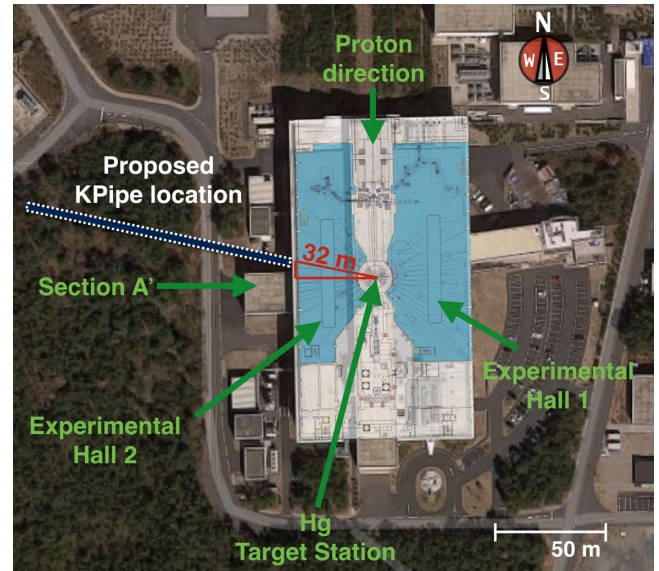

FIG. 1 (color online). An aerial view from Google Maps (2015) of the Materials and Life Science Experimental Facility layout with a superimposed schematic drawing [30] of the first floor, including the target station. The proposed KPipe location (shown with a dotted contour) is 32 m from the target station and 102° with respect to the incident proton beam direction. The detector extends radially outward from the target station.

goal of the KPipe detector design is to efficiently identify these 236 MeV ν_μ CC events, broadly characterized by two separated flashes of light in time coming from the prompt $\mu^- X$ followed by the muon's decay electron.

The KPipe design calls for a relatively low cost, 3 m inner diameter steel-reinforced, high density polyethylene (HDPE) pipe that is filled with liquid scintillator. As shown in Fig. 1, the pipe is positioned so that it extends radially outward from the target station. The upstream location maximizes the sensitivity to oscillations by being the shortest possible distance from the source, given spatial constraints. We have found that a long detector (120 m, 684 tons) is most suitable for optimizing sensitivity to oscillations across a wide range of the most pertinent parameter space, in consideration of current global fit results, the neutrino energy, $1/R^2$, and estimated cost.

The interior of the pipe contains a cylinder, constructed with an assembly of highly reflective panels, that optically separates the active volume from the cosmic ray (CR) veto. Hoops of inward-facing Silicon photomultipliers (SiPMs) are mounted on the interior of the panels. There are 100 equally spaced SiPMs per hoop, and each hoop is separated longitudinally by 10 cm (see Fig. 2). The space surrounding the inner target region on the other side of the panels is the 10 cm-thick veto region. The surfaces of the veto region are painted white, or lined with a Tyvek®-like material, for high reflectivity. Along the innermost side of the veto region are 120 hoops of outward-facing SiPMs that each run along the circumference of the pipe. The hoops have
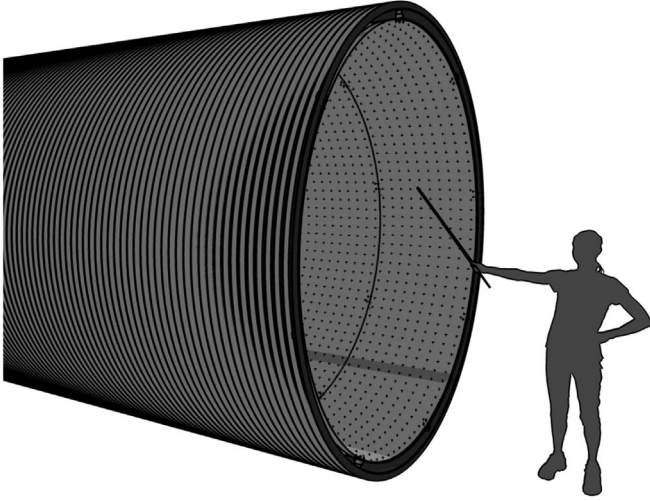
FIG. 2. The KPipe detector design, featuring a 3 m inner diameter HDPE vessel filled with liquid scintillator. SiPMs are seen mounted on the interior panels in hoops spaced by 10 cm in the longitudinal direction. The CR veto is a 10 cm space between the panels and the outer HDPE wall.

100 SiPMs each and are positioned at 1 m spacing along the inside of the veto region. The 10 cm spaces at the ends of the pipe are also instrumented. Each veto end cap is instrumented with 100 SiPMs that all face axially outward and are spaced equally apart on a circle with 1 m radius.

SiPMs are employed in both the target and veto regions because of their compact size and reduced cost when purchased in bulk. Currently available SiPMs typically have a quantum efficiency around 30%. In order to further reduce cost, we plan on multiplexing the SiPM channels. For the target region, each channel of readout electronics monitors 25 out of the 100 total SiPMs on a hoop. For the veto region, one channel monitors one side or end cap hoop. The active area of a SiPM can range from 1×1 mm^2 to about 6×6 mm^2. Assuming 6×6 mm^2 SiPMs, with 1200 hoops containing 100 SiPMs each, the target region will have a photocathode coverage of only $\sim 0.4\%$. Despite this low coverage, simulations of the experiment described in the next section indicate that there are an adequate number of SiPMs to achieve the goals of the experiment.

The KPipe detector succeeds despite the sparse amount of instrumentation in the inner region because of its use of liquid scintillator as the detector medium. The low photocathode coverage is overcome by the large amount of light produced by the scintillator per unit of energy deposited. Scintillators under consideration for KPipe include those based on mineral oil and linear alkylbenzene (LAB). One example of a currently deployed mineral oil-based scintillator is the one used by the NOνA experiment [39]. This scintillator is a mixture of 95%-by-mass mineral oil with 5% pseudocumene (1,2,4-trimethylbenzene) along with trace amounts of PPO (2,5-diphenyloxazole) and bis-MSB [1,4-Bis(2-methylstyryl)benzene] wavelength

shifters [40]. The UV photons emitted by the pseudocumene excite the PPO, which, as the primary scintillant, reemits in the range of 340–380 nm. These photons are then absorbed by the bis-MSB and reemitted in the 390–440 nm range. Along with developing their scintillator, the NOνA experiment has also established the methods to manufacture large quantities of it at a relatively low cost. Other examples of mineral oil-based scintillators are those offered by Saint-Gobain. For reference, the light yield of these scintillators ranges from 28% to 66% of anthracene or ~ 4500 to ~ 11400 photons/MeV [41]. Besides mineral oil, another option is to use a LAB-based liquid scintillator, similar to that being used by the SNO + experiment [42]. This liquid scintillator consists of the LAB as solvent with PPO acting as the wavelength shifter. The advantage of a LAB-based liquid scintillator over those based on mineral oil is that it has a comparable light yield to the brighter Saint-Gobain scintillators [43] while also being less toxic. In order to be conservative, we assume in simulations of the KPipe detector (discussed in the next section) a light yield consistent with the dimmest mineral oil-based liquid scintillator from Saint-Gobain (4500 photons/ MeV). The liquid scintillator that is eventually employed for KPipe will be some optimization between light yield, cost, and safety.

III. SIMULATION OF THE EXPERIMENTAL SETUP

In order to study the performance capabilities of KPipe, we have created simulations of both the neutrino source and the detector. The source simulations, using both GEANT4 [44] and MARS15 [45], model 3 GeV kinetic energy protons hitting the mercury target. The resulting particles are propagated, and the kinematics of all the neutrinos produced are recorded. Even though the majority (86%) of 236 MeV ν_μ are found to originate within the mercury target, a semirealistic geometry that incorporates the major components of the target and surrounding material is employed with GEANT4. About 75% of the K^+ are found to DAR within 25 cm of the upstream end of the mercury target and the ratio of ν_μ from K^+ DAR to ν_μ from K^+ decay in flight over 4π is $\sim 13:1$. The K^+ production rate varies depending on which simulation software is used. The GEANT4 model calculates the 236 MeV ν_μ yield to be 0.0038 ν_μ per POT, whereas the MARS15 model predicts 0.0072 ν_μ/POT. Later, when calculating the sensitivity of the experiment in Sec. V, we quote a sensitivity which relies on the MARS15 model for kaon production, as it has been more extensively tuned to data than GEANT4 [46].

The ν_μ flux is propagated to the KPipe detector whose closest end to the source is 32 m away. The ν_μ flux for $-0.25 < \cos\theta_z < -0.16$, where θ_z is the neutrino angle with respect to the proton direction $(+z)$, representative of the full detector length, is shown in Fig. 3 (left). The time

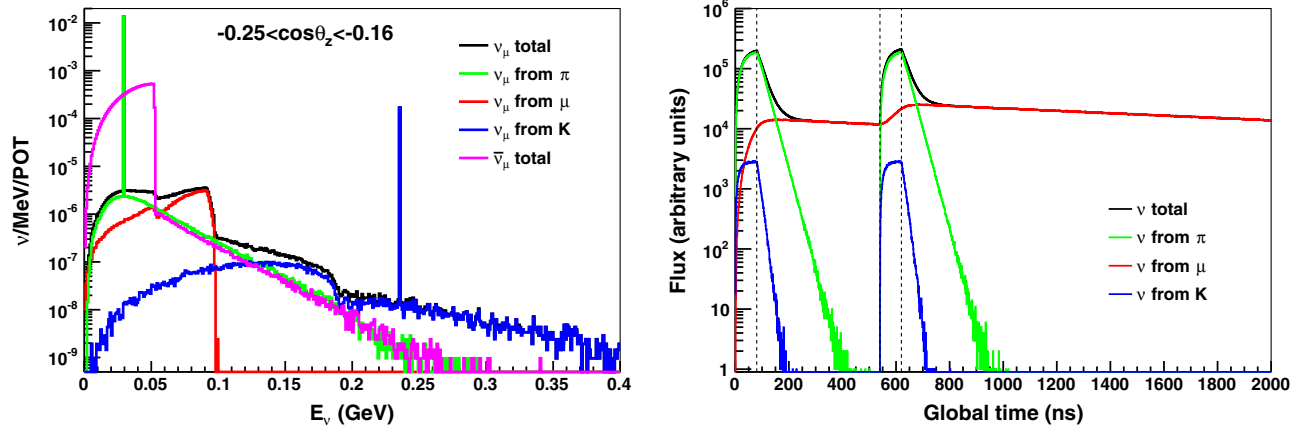FIG. 3 (color online).   Left: The muon neutrino and antineutrino flux with $-0.25 < \cos\theta_z < -0.16$, representative of the full detector length, where θ_z is the neutrino angle with respect to the proton direction $(+z)$. Right: The neutrino creation time relative to the two beam pulses (dotted lines). This distribution includes neutrinos emitted over all solid angles and energies.

distribution of all neutrinos coming from the source is shown in Fig. 3 (right). The two 80 ns wide proton pulses can be seen in the figure, while the blue histogram shows the neutrinos coming from kaon decay.

The interactions of neutrinos with the detector and surrounding materials are modeled with the NuWro event generator [47], and the ν_μ CC cross section and expected rate can be seen in Fig. 4. Notably, the signal (KDAR) to background (non-KDAR) ratio is 66:1 integrated over all energies. The high KDAR to non-KDAR ratio occurs, despite the large flux of low energy neutrinos, because of the muon production threshold (105.7 MeV) and small low energy cross section for CCQE interactions. In other words, if a neutrino-induced muon is observed, there is a 98.5% chance that it came from a 236 MeV ν_μ CC interaction. Given 5000 hours/year of J-PARC 1 MW operation $(3.75 \times 10^{22}$ POT/year), consistent with Ref. [48], we

expect 1.02×10^5 KDAR ν_μ CC events/year in the 684 ton active volume.

For each generated 236 MeV ν_μ CC interaction on carbon, NuWro provides the momentum of the outgoing muon and any final state nucleons (typically a single proton). Figure 5 shows the kinetic energies of the resulting KDAR signal muons along with the non-KDAR muons. The ν_μ CC cross section on carbon at 236 MeV according to NuWro and employed for the event rate estimate here is 1.3×10^{-39} cm^2/neutron. This is consistent with the random phase approximation (RPA) model's [49–51] cross section prediction of $(1.3 + 0.2) \times 10^{-39}$ cm^2/neutron (RPA QE + npnh). While NuWro is the only generator we use to produce simulated events, we did compare the kinematic distributions given by NuWro to those provided by GENIE [52] and the Martini *et al.* RPA model [51], which includes multinucleon effects.
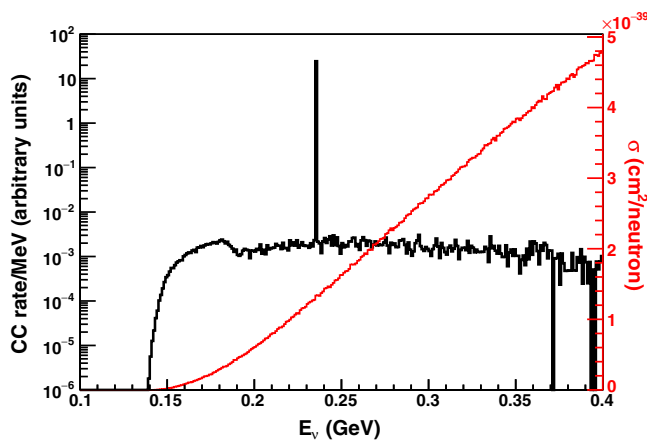

FIG. 4 (color online).   The ν_μ charged current event rate, for neutrinos with $-0.25 < \cos\theta_z < -0.16$, along with the employed ν_μ CC cross section. The monoenergetic 236 MeV neutrino signal is clearly visible above the background non-monoenergetic events, mainly coming from kaon decay in flight.
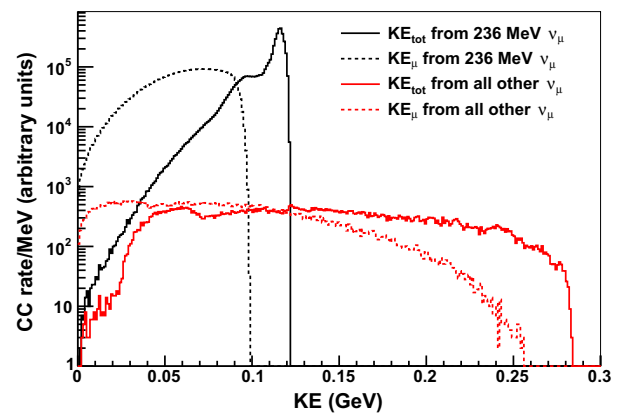

FIG. 5 (color online).   The muon and total kinetic energy $(\mathrm{KE_{tot}} = \mathrm{KE}_\mu + \sum \mathrm{KE_p})$ for the signal 236 MeV ν_μ charged current events compared to all other ν_μ. Only neutrinos with $-0.25 < \cos\theta_z < -0.16$ are considered. The ratio of integrated signal (black) to background (red) is 66:1.

Particle propagation through the detector is modeled using the GEANT4-based simulation package RAT [53]. The detector geometry input into the simulation is as described in the previous section. The detector is assumed to be on the surface and is surrounded by air only. Neutrino events in the detector are generated by first compiling a list of interactions using the energy distribution from the flux model described above and the NuWro generator. The position of the neutrino interactions is then distributed over a 5 m × 5 m × 140 m box that fully contains the 120 m long, 3 m in diameter cylindrical detector. The distribution of events in the box is weighted to take into account the $1/R^2$ dependence of the flux along with the density of the various materials in the simulation. The small divergence in the neutrino direction due to a point source is also considered. The RAT package includes a model for scintillator physics that derives from models previously employed by other liquid scintillator experiments such as KamLAND. The processes that are considered include scintillation, absorption, and reemission. All three have wavelength dependence. The reflectivity of surfaces in the detector is simulated using the models built into GEANT4.

In addition to the simulation of KDAR neutrino interactions with the detector and surrounding material, we simulate the propagation of CR throughout the volume. We use the simulation package CRY [54] to study the CR particle flux, which generates showers consisting of some combination of one or more muons, pions, electrons, photons, neutrons, or protons. The dark rate of SiPMs is also included in the simulation of the SiPM response. We use a dark rate of 1.6 MHz for each of the 130, 200 6 mm × 6 mm SiPMs (0.4% photo coverage) along with a total quantum efficiency of 30%. The dark rate comes from the specification for SenSL series C SiPMs which have an advertised dark rate of $< 100,000$ Hz/mm^2 [55].

IV. ISOLATING AND RECONSTRUCTING ν_μ EVENTS FROM THE KDAR SOURCE

Signal events from the KDAR neutrino source are identified by the observation of two sequential pulses of light. The prompt signal comes from the muon and vertex energy deposition. The delayed signal is from the Michel electron produced by the decay of the muon ($\nu_\mu {}^{12}C \rightarrow \mu^- X, \mu^- \rightarrow e^- \nu_\mu \bar{\nu}_e$). We apply a pulse finding algorithm to identify both light signals from the SiPMs. The algorithm uses a rolling 20 ns window over which the number of hits in the SiPMs is summed and the expected dark hit contribution in the window is subtracted. The prompt signal is found when the hit sum with subtraction is above a given threshold, specifically one that is four times larger than the standard deviation of the expected number of dark hits. After the prompt signal is found, the algorithm searches for the Michel signal using the same method, except that the threshold is raised to account for both the expected dark noise and the contribution of SiPM hits from
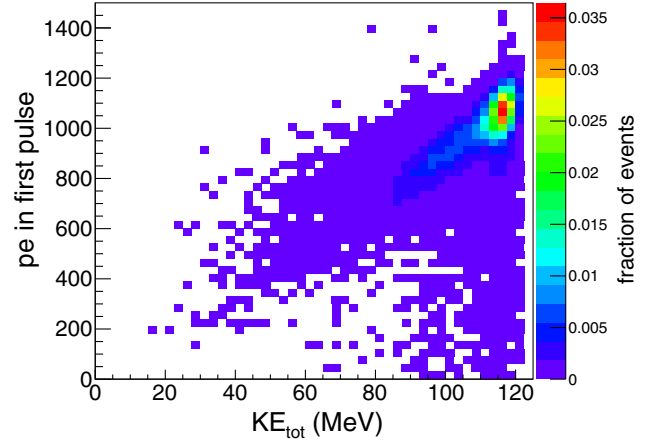

FIG. 6 (color online). The number of photoelectrons in a 236 MeV ν_μ CC event's prompt signal versus the total kinetic energy ($KE_{tot} = KE_\mu + \sum KE_p$).

the prompt signal. This expected hit contribution is dictated by the decay time of the scintillator. After isolating coincident signals, the position along the detector of both the primary interaction and Michel signal is determined by the photoelectron-weighted position of the hits seen by the SiPMs. Using the position of the prompt signal, we find that the vertex position resolution of the interaction is 80 cm. The current proposed readout is likely unable to reconstruct more detailed information about the event such as the muon angle, although this information is not necessary for KPipe's primary measurement.

Figure 6 shows the number of photoelectrons (pe) in the prompt signal as a function of total kinetic energy, KE_{tot}, defined as the total kinetic energy of the muon and any final state protons ($KE_{tot} = KE_\mu + \sum KE_p$). The figure shows simulated data from 236 MeV KDAR ν_μ CC interactions. The prompt signal usually contains over 800 pe, indicating that, despite the low photocathode coverage, the amount of observed light for the signal events is high enough for efficient reconstruction. Further, the figure shows that KE_{tot} correlates well with the number of pe seen. Using the peak of this distribution, the detector light yield is calculated to be 9.2 pe/MeV, which includes effects from quantum efficiency, photocathode coverage, and absorption.

A. Isolating the signal

The primary background to the ν_μ CC signal events comes from stopping cosmogenic muons in the detector. We envision applying the following selection requirements in order to select signal interactions and reject CR backgrounds:

(1) the prompt signal occurs within 125 ns windows following each of the two 80 ns beam pulses,
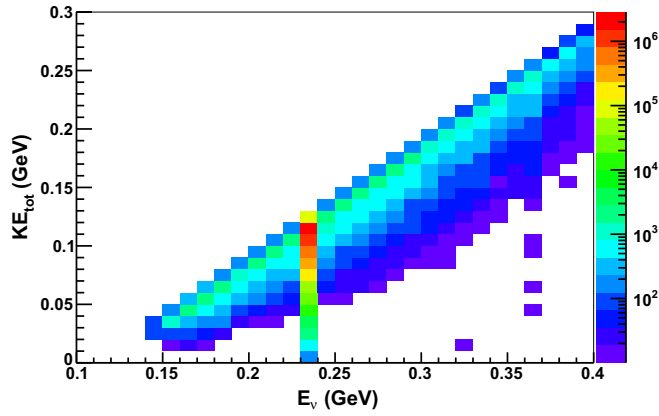(2) the prompt signal has a reconstructed energy in the range $22 < E_{vis} < 142$ MeV ($200 < pe < 1300$),

FIG. 7 (color online). The total kinetic energy ($KE_{tot} = KE_\mu + \sum KE_p$) versus the energy of neutrinos from CC interactions in KPipe. Only neutrinos with $-0.25 < \cos\theta_z < -0.16$ are considered. The Z-axis units are arbitrary.

   (3) the delayed signal occurs within 10 μs of the prompt signal,
   (4) the delayed signal reconstructed visible energy is $11 < E_{vis} < 82$ MeV ($100 < pe < 750$),
   (5) the distance between the prompt and delayed signal is less than 1.5 m, and
   (6) the summed signal height in the ten nearest veto SiPM hoops to the prompt signal is less than four times the dark rate σ within a 125 ns window after the start of each 80 ns beam pulse.

Note that for the cuts on visible energy, E_{vis}, the corresponding values in *pe* are given in parentheses. These are the values used in the Monte Carlo study of the KDAR signal efficiency and CR background rejection.

The first cut (1) takes advantage of the pulsed proton beam. Accepting events only within a 125 ns window after each 80 ns proton pulse efficiently selects 99.9% of the KDAR neutrinos while removing many of the events coming from other neutrino sources. The small 125 ns event window also limits the rate of CR events even before the other selection cuts are applied. According to the simulation, CR particles create at least one detectable flash in either the target region or veto in only 0.87% of all windows.

The second cut (2) utilizes the fact that, because the signal events come from monoenergetic neutrinos, the energy of the outgoing particles falls in a fairly narrow range. Figure 7 shows the total kinetic energy of the muons and any final state protons, KE_{tot}, as a function of neutrino energy for ν_μ CC events in the detector. The upper bound of 142 MeV ensures that the signal neutrino events are preserved with high efficiency, while removing non-KDAR muon neutrinos at higher energies. More importantly, the upper bound removes bright CR events. Based on the simulation, 72% of all detectable CR events (i.e. ones that produce one or more detected flashes) are removed by the high energy cut, many of which are through-going muons.

Along with kaon decay-in-flight neutrinos, the low energy bound also removes all relevant backgrounds from CR-induced spallation products and is well above the visible energy from radiogenic backgrounds. With both a high and low energy cut on the prompt signal, 87% of all CR events are removed.

The cuts related to Michel electron timing, energy, and spatial coincidence (cuts 3–5) are chosen to efficiently retain signal while removing most of the in-time through-going CR muons that traverse the detector, as well as other backgrounds. A coincident signal coming from nonstopping muons can occur due to a CR shower with two or more particles or an associated muon spallation-induced isotope. The timing, energy, and spatial cuts on the Michel candidate reduce much of this coincident background. Applying the above cuts along with the Michel signal cuts reduces the CR rate to 750 Hz, which means that only 0.01% of all signal windows will contain a CR event. At this stage in the cuts, less than two percent of detectable CR events remain.

The final cut (6) applied removes all events that create a flash of light in the veto. The veto is only 10 cm thick and is more sparsely instrumented than the target region. However, enough light is produced that the veto is able to reject 99.5% of all detectable CR events with at least one muon. We find that lining the walls of the veto with a highly reflective material plays an important role in the veto performance. With all cuts applied, we estimate that the rate of CR events is 27 Hz over the entire active volume. A large sample of CR events, including Michel electrons, can be collected in order to calibrate the detector, study efficiency of the above cuts, and measure the rate of CR events that pass.

In addition to CR backgrounds and non-KDAR muon neutrino events, an additional coincident background can come from beam-induced neutron interactions that produce a Δ^+ in the detector that subsequently decays into a π^+. The latter can then stop and decay to a muon followed by a Michel electron. We assume that this background is negligible for this study. All in-time beam-related backgrounds will be measured before deploying KPipe, and adequate shielding will be installed in order to mitigate them.

Overall, our studies indicate that the dominant background is from CR shower events that are not removed by the above cuts. Of the 27 Hz rate that passes, the simulations show that 70% of the rate is due to stopping muons. The remaining 30% is due to showers involving photons, electrons, and neutrons. In the simulation, we do not include any additional passive shielding, for example coming from overburden. If the detector is buried or shielded, we expect these nonmuon backgrounds to be further reduced. The CR background should be distributed uniformly throughout the detector and can be measured precisely using identified out-of-time stopped muons. As a

result, only the statistical error from the total number of background events expected to pass the cuts is included in the sensitivity analysis, described in Sec. V.

B. Detection efficiency

The cuts introduce inefficiency in the signal. We assume that the neutrino events are distributed evenly in radius and fall as $1/R^2$ throughout the detector. Signal events near the lateral edge of the target region can exit the detector before the muon can decay. This leads to an acceptance that is a function of radius. Based on an active detector radius of 1.45 m, we find an acceptance of 87% with respect to KDAR ν_μ CC interactions whose true vertex is in the target region. The selection cuts described above are 89% efficient according to the simulation. This includes events where the muon is captured by the nucleus, which occurs in the target region 6% of the time. For a subset of these events, there is also an additional 0.75% dead-time loss due to the rate of CR events in the veto.

In summary, the total efficiency for all signal events is 77%, leading to an expected total KDAR ν_μ CC rate of 7.8×10^4 events distributed along the pipe's active volume per year of running. This is on average 4.9×10^{-5} KDAR events per proton beam window without oscillations. This compares with 3.4×10^{-6} CR events per proton beam window. In the most upstream 1 m of the detector, the unoscillated signal to background ratio is about 60∶1; in the most downstream 1 m of the detector, the unoscillated signal to background ratio is about 3∶1.

V. SENSITIVITY

The expected number of ν_μ events as a function of distance is determined numerically for a no-oscillation hypothesis using the CC cross section, ν_μ production rate, detector up time, and total efficiency (values shown in

TABLE I.   Summary of the relevant experimental parameters.

| Parameter	Value
Detector length	120 m
Active detector radius	1.45 m
Closest distance to source	32 m
Liquid scintillator density	0.863 g/cm^3
Active detector mass	684 tons
Proton rate (1 MW)	3.75×10^{22} POT/year
KDAR ν_μ yield (MARS15)	0.0072 ν_μ/POT
ν_μ CC σ @ 236 MeV (NuWro)	1.3×10^{-39} cm^2/neutron
Raw KDAR CC event rate	1.02×10^5 events/year
KDAR signal efficiency	77%
Vertex resolution	80 cm
Light yield	4500 photons/ MeV
ν_μ creation point uncertainty	25 cm
Cosmic ray background rate	27 Hz
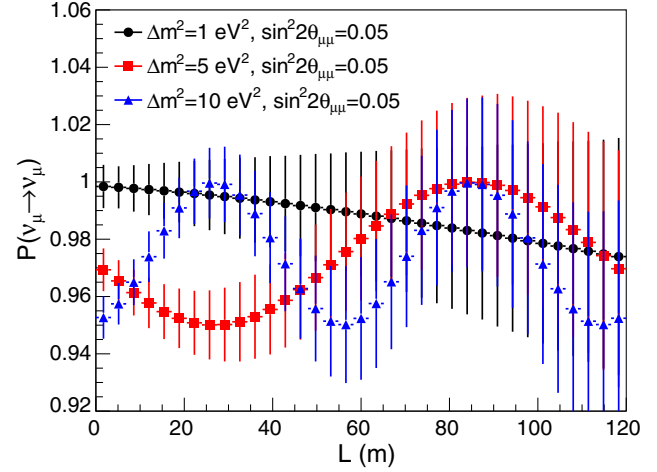
FIG. 8 (color online).   Three sample oscillation probability measurements as a function of L for three years of running. The error bars incorporate statistical uncertainties of both the ν_μ signal and the cosmic ray background. The equivalent range of observable L/E corresponds to 0.14 to 0.64 m/MeV.

Table I). First, events are generated in the detector with a given energy and position. Each event is then oscillated according to Eq. (3) and smeared to incorporate the baseline uncertainties coming from the neutrino creation point and the position reconstruction. The oscillation probabilities for three different Δm^2 values $(1, 5, 10 \text{ eV}^2)$ can be seen in Fig 8. The error bars correspond to the statistical uncertainty associated with a three year ν_μ measurement with a CR rate of 27 Hz. This background rate corresponds to 132 CR events that pass our selection cuts for each 1 m slice of the detector.

The sensitivity of the experiment is evaluated using a shape-only χ^2 statistic similar to that described in Ref. [56]. However, we replace the covariance matrix with the Neyman χ^2 convention, since we do not include any correlated systematic uncertainties between each L/E bin. Using Eq. (3) for the oscillation probability, the χ^2 value at each pair of oscillation parameters, Δm^2 and $U_{\mu 4}$, is calculated by comparing the no-oscillation signal $(N_i^{\nu,\mathrm{un}} + N_i^{\mathrm{bkgd}})$ to the oscillation signal $(N_i^{\nu,\mathrm{osc}} + N_i^{\mathrm{bkgd}})$ in each L/E bin, i. Here, $N_i^{\nu,\mathrm{un}}$ and $N_i^{\nu,\mathrm{osc}}$ are defined as the number of expected ν_μ events in bin i given a no-oscillation prediction and an oscillation prediction, respectively. The number of events in a bin due to background is then added to the ν_μ prediction. The ΔL value used in setting the bin size is 80 cm. Defining for each ith L/E bin the difference between the no-oscillation and oscillation signal, n_i, where

$$n_i = (N_i^{\nu,\mathrm{un}} + N_i^{\mathrm{bkgd}}) - (\xi N_i^{\nu,\mathrm{osc}} + N_i^{\mathrm{bkgd}}), \quad (4)$$

the χ^2 is then

$$\chi^2 = \sum_i^{nbins} \frac{n_i^2}{N_i^{\nu,un} + N_i^{bkgd}}. \tag{5}$$

The normalization constant, ξ, in Eq. (4), is included in order to make the analysis shape only and is constrained to be

$$\xi = \frac{\sum_i N_i^{\nu,un}}{\sum_i N_i^{\nu,osc}}. \tag{6}$$

For the 90% confidence limit reported, a one degree of freedom, one-sided raster scan threshold of $\chi^2 = 1.64$ is used. The 5σ threshold is $\chi^2 = 25.0$, considering a one degree of freedom, two-sided raster scan.

For the subsequent sensitivity plots, the oscillation prediction, $N_i^{\nu,osc}$, has been simplified by the two flavor approximation to the $3 + 1$ neutrino oscillation model [Eq. (3)], where we define $\sin^2(2\theta_{\mu\mu}) = 4|U_{\mu4}|^2(1-|U_{\mu4}|^2)$.

The KPipe search for sterile neutrinos, which uses only the relative rate of events along the pipe, is helped by the fact that uncertainties associated with the absolute normalization of the event rate expectation are not relevant for this shape-only analysis. This includes theoretical uncertainties in the kaon production and neutrino cross section. Instead, the dominant uncertainty associated with the weight of each bin comes from the combined statistical uncertainty of the ν_μ measurement and the CR background. In the sensitivity studies, we assume a CR background rate of 27 Hz over the entire detector. Further, there are two uncertainties associated with the neutrino baseline L: the creation point of the ν_μ from the decaying K^+ has an uncertainty of 25 cm; the reconstructed position resolution, described in Sec. IV, has an uncertainty of 80 cm. There is no uncertainty associated with the energy reconstruction since the ν_μ have a definite energy. We also include a total detection efficiency due to the selection cuts, dead-time, and escaping muons described in Sec. IV A of 77%. A summary of the relevant experimental parameters and assumptions can be seen in Table I.

Figure 9 shows the projected 90% and 5σ sensitivity of KPipe to $\nu_\mu \to \nu_\mu$ for three years of running. The global fit allowed regions, given in red, were produced using a new software package based on the previous work of Ignarra *et al.* [11]. We refer to this work as Collin *et al.* [57]. The fit includes the data sets described in Ref. [58] with the exception of the atmospheric limit. The model parameters are explored using a Markov chain Monte Carlo algorithm. Contours are drawn in a two-dimensional parameter space using two degrees of freedom χ^2 values for 90% and 99% probability. After three years of KPipe running, the 5σ exclusion contour covers the best fit point at $\Delta m^2 = 0.93$ eV^2 and $\sin^2(2\theta_{\mu\mu}) = 0.11$.

Figure 10 shows a comparison between KPipe's predicted six year 90% sensitivity and the predicted sensitivity
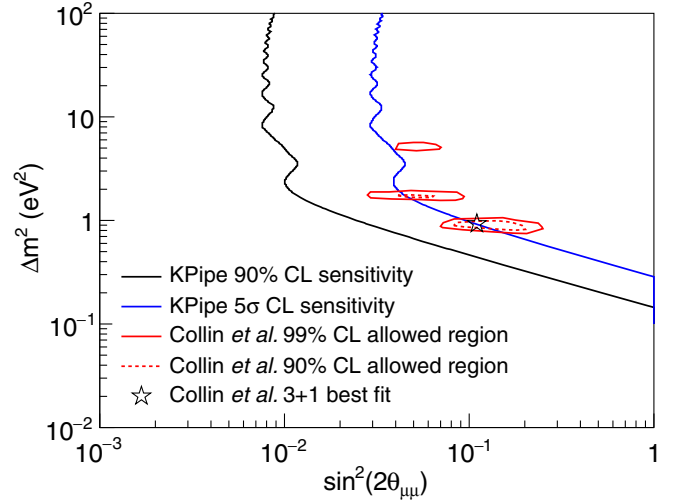

FIG. 9 (color online). The projected sensitivity of KPipe to muon neutrino disappearance with three years of running, including the cosmic ray background, signal efficiencies, and reconstruction uncertainties described in the text. The red contours are the global allowed regions given by Collin *et al.* [57].

of SBN [31] assuming 6.6×10^{20} POT (three years) in SBND and the ICARUS-T600 and 13.2×10^{20} POT (six years) in MicroBooNE. The dashed contour represents the combined 90% excluded region based on the muon neutrino disappearance results of MiniBooNE and SciBooNE [17]. SBN and KPipe have similar sensitivity reach in the $\Delta m^2 = 1$–4 eV^2 region; however SBN performs better at low Δm^2 and KPipe at high Δm^2; the complementarity between the experiments is clear.
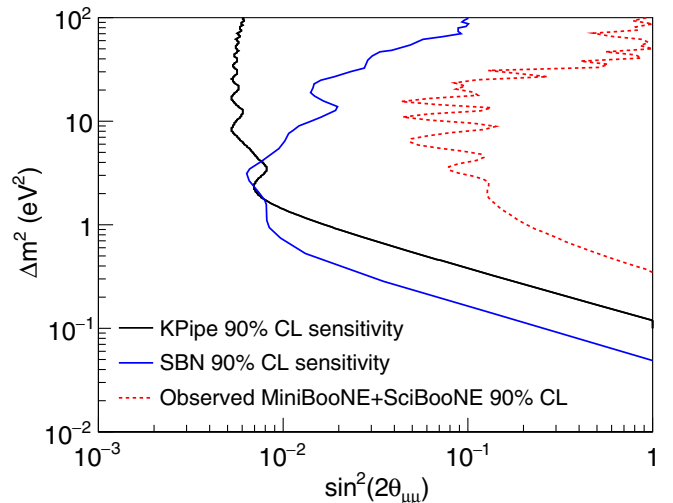

FIG. 10 (color online). The 90% C.L. sensitivity of KPipe with six years of running, compared to the sensitivity from six years of the SBN program. The KPipe sensitivity estimate includes the cosmic ray background, signal efficiencies, and reconstruction uncertainties described in the text.

VI. CONCLUSION

The J-PARC MLF facility provides a unique and intense source of neutrinos in the form of monoenergetic 236 MeV muon neutrinos coming from the decay at rest of positively charged kaons. The KPipe experiment seeks to take advantage of this source for a decisive ν_μ disappearance search at high Δm^2 in order to address the existing anomalies in this parameter space. The 120 m long, 3 m in diameter liquid scintillator based active volume (684 ton) will feature 0.4% photo coverage for detecting these ν_μ CC events in an attempt to discern an oscillation wave along the length of the detector.

In contrast to other neutrino sources, the KPipe neutrinos are dominantly monoenergetic. This provides a great advantage in searching for neutrino oscillations. A neutrino (or antineutrino) induced double-coincidence muon signal detected with KPipe has a 98.5% chance of being from a 236 MeV ν_μ CC event. This simple fact allows the active detector requirements to be extremely modest, the systematic uncertainties to be practically eliminated, and the detector's energy resolution to be only a weak consideration.

Within three years of running, KPipe will be able to cover the current global fit allowed region to 5σ. The sensitivity for a six year run at the J-PARC facility will enhance existing single experiment limits on ν_μ disappearance by an order of magnitude in Δm^2. Such a measurement, when considered alone, or in combination with existing and proposed electron flavor disappearance and appearance measurements, can severely constrain models associated with oscillations involving one or more light sterile neutrinos.

[1] A. Aguilar *et al.* (LSND Collaboration), Phys. Rev. D **64,** 112007 (2001).

[2] A. A. Aguilar-Arevalo *et al.* (MiniBooNE Collaboration), Phys. Rev. Lett. **102,** 101802 (2009).

[3] A. A. Aguilar-Arevalo *et al.* (MiniBooNE Collaboration), Phys. Rev. Lett. **110,** 161801 (2013).

[4] G. Mention, M. Fechner, T. Lasserre, T. A. Mueller, D. Lhuillier, M. Cribier, and A. Letourneau, Phys. Rev. D **83,** 073006 (2011).

[5] C. Zhang, X. Qian, and P. Vogel, Phys. Rev. D **87,** 073018 (2013).

[6] M. A. Acero, C. Giunti, and M. Laveder, Phys. Rev. D **78,** 073009 (2008).

[7] C. Giunti and M. Laveder, Phys. Rev. C **83,** 065504 (2011).

[8] J. N. Abdurashitov *et al.* (SAGE Collaboration), Phys. Rev. C **80,** 015807 (2009).

[9] F. Kaether, W. Hampel, G. Heusser, J. Kiko, and T. Kirsten, Phys. Lett. B **685,** 47 (2010).

[10] M. Sorel, J. M. Conrad, and M. Shaevitz, Phys. Rev. D **70,** 073004 (2004).

[11] J. M. Conrad, C. M. Ignarra, G. Karagiorgi, M. H. Shaevitz, and J. Spitz, Adv. High Energy Phys. **2013,** 1 (2013).

[12] J. Kopp, P. A. N. Machado, M. Maltoni, and T. Schwetz, J. High Energy Phys. 05 (2013) 050.

[13] C. Giunti and M. Laveder, Phys. Lett. B **706,** 200 (2011); Phys. Rev. D **84,** 073008 (2011).

[14] B. Armbruster *et al.* (KARMEN Collaboration), Phys. Rev. D **65,** 112001 (2002).

[15] G. Cheng *et al.* (MiniBooNE and SciBooNE Collaborations), Phys. Rev. D **86,** 052009 2012.

[16] J. M. Conrad and M. H. Shaevitz, Phys. Rev. D **85,** 013017 (2012).

[17] K. B. M. Mahn *et al.* (SciBooNE and MiniBooNE Collaborations), Phys. Rev. D **85,** 032007 (2012).

[18] P. Adamson *et al.* (MiniBooNE Collaboration), Phys. Rev. Lett. **102,** 211801 (2009).

[19] P. Astier *et al.* (NOMAD Collaboration), Phys. Lett. B **570,** 19 (2003); D. Gibin, Nucl. Phys. B, Proc. Suppl. **66,** 366 (1998); V. Valuev (NOMAD Collaboration), Proc. Sci. HEP2001 (**2001**) 190.

[20] I. Stockdale *et al.* (CCFR Collaboration), Phys. Rev. Lett. **52,** 1384 (1984); Z. Phys. C **27,** 53 (1985).

[21] F. Dydak *et al.*, Phys. Lett. **134B,** 281 (1984).

[22] M. Maltoni, T. Schwetz, M. A. Tortola, and J. W. F. Valle, New J. Phys. **6,** 122 (2004).

[23] J. Hamann, S. Hannestad, G. G. Raffelt, and Y. Y. Y. Wong, J. Cosmol. Astropart. Phys. 09 (2011) 034.

[24] K. Abazajian *et al.*, arXiv:1204.5379.

[25] S. Axani *et al.* http://dspace.mit.edu/handle/1721.1/98388, 2015.

[26] A. Bungau *et al.*, Phys. Rev. Lett. **109,** 141802 (2012).

[27] J. Ashenfelter *et al.*, arXiv:1309.7647.

[28] C. Lane *et al.*, arXiv:1501.06935.

[29] G. Bellini *et al.*, J. High Energy Phys. 08 (2013) 038.

[30] M. Harada *et al.*, arXiv:1310.1437.

[31] R. Acciarri *et al.* (ICARUS-WA104, LAr1-ND, Micro-BooNE Collaborations), arXiv:1503.01520.

[32] A. J. Anderson, J. M. Conrad, E. Figueroa-Feliciano, C. Ignarra, G. Karagiorgi, K. Scholberg, M. H. Shaevitz, and J. Spitz, Phys. Rev. D **86,** 013004 (2012).

[33] M. Elnimr *et al.*, arXiv:1307.7097.

[34] J. M. Conrad and M. H. Shaevitz, Phys. Rev. D **89**, 057301 (2014).

[35] J. Beringer *et al.* (Particle Data Group), Phys. Rev. D **86**, 010001 (2012).

[36] J. Spitz, Phys. Rev. D **85**, 093020 (2012).

[37] J. Spitz, Phys. Rev. D **89**, 073007 (2014).

[38] J-PARC Project Newsletter special issue, May 2015; http://j-parc.jp/hypermail/news-l.2015/0003.html.

[39] D. Ayres *et al.* (NOνA Collaboration), arXiv:hep-ex/0503053.

[40] S. Mufson *et al.*, Nucl. Instrum. Methods Phys. Res., Sect. A **799**, 1 (2015).

[41] Saint-Gobain, http://www.crystals.saint-gobain.com/Liquid_scintillators.aspx, 2015.

[42] H. M. O'Keeffe, E. O'Sullivan, and M. C. Chen, Nucl. Instrum. Methods Phys. Res., Sect. A **640**, 119 (2011).

[43] H. W. C. Tseung, J. Kaspar, and N. Tolich, Nucl. Instrum. Methods Phys. Res., Sect. A **654**, 318 (2011).

[44] S. Agostinelli *et al.*, Nucl. Instrum. Methods Phys. Res., Sect. A **506**, 250 (2003); Geant4 version 4.9.6p04 is used with the QGSP_BERT physics list.

[45] N. V. Mokhov, Report No. FERMILAB-FN-628, 1995; O. E. Krivosheev and N. V. Mokhov, MARS code status, Report No. Fermilab-Conf-00/181, 2000; O. E. Krivosheev and N. V. Mokhov, Status of MARS Code, Report No. Fermilab-Conf-03/053, 2003; N. V. Mokhov, K. K. Gudima, C. C. James *et al.*, Recent enhancements to the MARS15 code, Report No. Fermilab-Conf-04/053, 2004; MARS1514 is used with the LAQGSM model.

[46] K. K. Gudima, N. V. Mokhov, and S. I. Striganov, Report No. Fermilab-Conf-09-647-APC, 2009.

[47] C. Juszczak, Acta Phys. Pol. B **40**, 2507 (2009); T. Golan, C. Juszczak, and J. Sobczyk, Phys. Rev. C **86**, 015505 (2012); NuWro version "11q" is used with a spectral function implementation.

[48] M. Harada *et al.*, arXiv:1502.02255.

[49] M. Martini, M. Ericson, G. Chanfray, and J. Marteau, Phys. Rev. C **80**, 065501 (2009).

[50] M. Martini, M. Ericson, and G. Chanfray, Phys. Rev. C **84**, 055502 (2011).

[51] M. Martini (private communication).

[52] C. Andreopoulos *et al.*, Nucl. Instrum. Methods Phys. Res., Sect. A **614**, 87 (2010).

[53] RAT, Public Edition, https://github.com/rat-pac/rat-pac.

[54] C. Hagmann, D. Lange, J. Verbeke, and D. Wright, Report No. UCRL-TM-229453, 2012.

[55] SensL, Series-C data sheet, http://www.sensl.com/downloads/ds/DS-MicroCseries.pdf, 2015.

[56] A. J. Franke, Ph.D. thesis, Columbia University, 2012.

[57] G. Collin, J. Conrad, and M. Shaevitz, Phys. Rev. D (to be published).

[58] C. M. Ignarra, Nucl. Phys. B, Proc. Suppl. **237**–**238**, 173 (2013).